10 One-photon two-electron transitions at surfaces

N. Fominykh, J. Berakdar[1], J. Henk, S. Samarin, A. Morozov, F. U. Hillebrecht, J. Kirschner, and P. Bruno

10.1 Introduction

The theoretical description of the behaviour of N interacting electrons moving in an external field implies the solution of a complicated many-body problem. An efficient, and in many cases adequate approach to this problem of interacting fermions has been provided by the effective field approach, i. e., by considering an individual particle to move independently in an effective field created by the average interaction with other particles. The Hartree-Fock scheme and the density functional theory within the local density approximation are prominent representatives for effective field procedures [1–3], which in general yield accurate predictions for a number of properties of materials. The limitations of these approaches become however evident when strongly correlated systems are considered, e. g., transition-metal oxides and heavy Fermion compounds [1].

In this work we focus on one of the tools to assess the effects of electronic correlations and the range of validity of effective field models. Generally speaking, one can expect the effective field approximation to break down whenever the strong short-range components of the electron-electron interaction are relevant. This is because in such an approach the electrons move independently from each other. This implies that the wavefunction contains a large portion of configurations, in which two electrons are so close to each other that they are exposed to the strong repulsive electron-electron interaction. In this situation, the concept of an effective, averaged field is clearly inadequate. In the realm of many-body theory a number of methods have been proposed to deal with this kind of correlation effects. Here we mention the Brueckner hole-line expansion [4–6], the 'exponential S' or coupled cluster method [7,8], quantum Monte-Carlo techniques [9, 10], and the Green's function method which we shall employ in the following. All these methods provide correlated many-body wavefunctions that account for the details of the inter-particle interaction. At the same time, the question arises which kind of experimental techniques are suitable to expose the effect of the short-distance electron-electron interaction and to assess the range of validity of various theoretical models.

To show the effect of correlation in a heuristic way let us consider the case of an infinite, homogeneous electron gas: The mean-field wavefunction is then a Slater determinant built out of plane-wave states, labeled by wavevectors k_i. All single-particle states with k_i smaller than the Fermi wavenumber k_F are occupied. Including correlations in this uncorrelated state leads to a partial depletion of some single-particle states with $k_i < k_F$ and a nonvanishing occu-

---

[1] Corresponding author.

pation of some states with higher wavenumbers. This simple example illustrates that a study of the high-momentum components in the single-particle wavefunctions has the potential to uncover the effects of short-range correlations. A way to investigate experimentally the high-momentum components is offered by measuring the coincident spectrum for the electron-pair emission upon electron impact, i. e., the (e,2e) experiment (one electron in, two electrons out). This kind of studies is reviewed by Feder and Gollisch in this book [11]. Another spectroscopic method for electronic correlation is the coincident, photon-induced electron-pair emission (γ,2e). This technique is even more sensitive to the effects of correlations than (e,2e) experiments. In fact, it can be shown that the cross section for (γ,2e) vanishes in absence of correlations [12]. Experimentally, the realization of the (γ,2e) process at surfaces has long been a challenge due to the low count rates (compared to single electron emission) which is inherent to coincidence studies. First experiments with a momentum resolution of the photo-electrons have been reported in Refs. [13, 14]. For atomic, molecular and nuclear matter the multi-particle coincidence technique is well established and has yielded a wealth of important information on the many-particle excitation dynamics. This information has been used to test various many-body theories (for recent reviews we refer to [15–20]). In this article we extend this multi-particle spectroscopy to solids and surfaces. A brief account is given on the theoretical and the experimental status of the photo-induced two-electron emission from surfaces. The formal theory and the current numerical implementations will be discussed and the results for the angular and the energy-correlation functions of the two photoelectrons will be presented and compared with presently available experimental data.

10.2   General considerations

This section provides the formal theoretical foundations and the calculational ingredients needed for a theoretical description of the (γ,2e) process. We also point out relation between the (γ,2e) and the (e,2e) reactions. There are a number of theoretical tools to deal properly with electronic correlations, however most of them, like the hole-line expansion and the coupled-cluster methods [3,21], are restricted to deal with ground-state properties. An appropriate framework for the treatment of (γ,2e) and (e,2e), which involves correlated excited states, is provided by the Green's function approach. This method offers an access to dynamic properties like, e. g., the single- and the two-particle spectral functions which are closely related to the cross section of single and two-particle emission [as produced by (e,2e) and (γ,2e) processes]. A general description of the Green's function approach can be found in various textbooks [21–25]. Here we focus on the aspects which are of immediate relevance to (γ,2e) and (e,2e).

10.2.1   The single-particle Green's function

The single-particle Green's function $g(\alpha t, \beta t')$ can be considered as an expectation value for the time-ordered product of two operators evaluated with respect to the correlated, exact ground-state $|\Psi_0\rangle$ of the N electron system (we assume $|\Psi_0\rangle$ to be properly normalized):

$$i\, g(\alpha t, \beta t') = \langle \Psi_0 | \mathcal{T}[a_{H\alpha}(t)\, a_{H\beta}^\dagger(t')] | \Psi_0\rangle, \tag{10.1}$$

where $\mathcal{T}$ is the time ordering operator. $a_{H\beta}^\dagger(t')$ and $a_{H\alpha}(t)$ stand respectively for the fermionic creation and annihilation operators in the Heisenberg picture represented in an appropriate basis, the members of which characterized by quantum numbers α and β. For a translationally invariant system, the appropriate basis states are the momentum eigenstates. The effect of the chronological operator $\mathcal{T}$ can be described in terms of the step function $\Theta(t - t')$, in which case the Green's function is given by

$$
\begin{aligned}
i g(k, t - t') &= \Theta(t - t')\langle \Psi_0 | a_{Hk}(t) a_{Hk}^\dagger(t') | \Psi_0\rangle \\
&\quad - \Theta(t' - t)\langle \Psi_0 | a_{Hk}^\dagger(t') a_{Hk}(t) | \Psi_0\rangle \\
&= \Theta(t - t') \sum_\gamma e^{-i\left[E_\gamma^{(N+1)} - E_0^{(N)}\right](t - t')} \left| \langle \Psi_\gamma^{(N+1)} | a_k^\dagger | \Psi_0\rangle \right|^2 \\
&\quad - \Theta(t' - t) \sum_\delta e^{-i\left[E_0^{(N)} - E_\delta^{(N-1)}\right](t - t')} \left| \langle \Psi_\delta^{(N-1)} | a_k | \Psi_0\rangle \right|^2 .
\end{aligned}
\tag{10.2}
$$

In this equation, $\Psi_\gamma^{(N+1)}$ and $\Psi_\delta^{(N-1)}$ denote a complete set of eigenstates of the $(N + 1)$- and the $(N - 1)$-particle system, respectively. The energies $E_0^{(N)}$, $E_\gamma^{(N+1)}$, and $E_\delta^{(N-1)}$ refer to the exact energies for the correlated ground state of respectively the N-, the $(N + 1)$-, and the $(N - 1)$-particle system. The exponential with the energies in Eq. (10.2) is due to the Hamiltonians in the exponential functions in the definition of the Heisenberg operators.

Noting that the step function has the integral representation

$$\Theta(t) = -\lim_{\eta \to 0} \frac{1}{2\pi i} \int_{-\infty}^{\infty} d\omega \frac{e^{-i\omega t}}{\omega + i\eta}, \tag{10.3}$$

the Green's function in energy space can be obtained via Fourier transforming the time difference $t - t'$ to the energy variable ω. This yields the spectral or Lehmann representation of the single-particle Green's function [26],

$$
g(k, \omega) = \lim_{\eta \to 0} \left[\sum_\gamma \frac{\left| \langle \Psi_\gamma^{(N+1)} | a_k^\dagger | \Psi_0\rangle \right|^2}{\omega - [E_\gamma^{(N+1)} - E_0^{(N)}] + i\eta} \right.
$$
$$
\left. + \sum_\delta \frac{\left| \langle \Psi_\delta^{(N-1)} | a_k | \Psi_0\rangle \right|^2}{\omega - [E_0^{(N)} - E_\delta^{(N-1)}] - i\eta} \right]. \tag{10.4}
$$

Relation (10.4) points out that the single-particle Green's function is representable in terms of measurable quantities: The poles of $g(k, \omega)$ correspond to the change in energy (with respect to $E_0^{(N)}$) if one particle is added ($E_\gamma^{(N+1)} - E_0^{(N)}$) or one particle is removed ($E_0^{(N)} - E_\delta^{(N-1)}$) from the reference ground state with N interacting particle. The residua of these poles are given by the *spectroscopic factors*, i. e., the measurable probabilities of adding and removing one particle with wavevector k to produce the specific state γ (δ) of the residual system. Clearly, the latter probability is of a direct relevance to the (e,2e) process. The infinitesimal

quantity η in Eq. (10.4) shifts the poles below the Fermi energy [the states of the $(N-1)$ system] to slightly above the real axis and those above the Fermi energy [the states of the $(N+1)$ system] to slightly below the real axis.

It is customary to write the spectral representation of the single-particle Green's function in terms of the hole and particle spectral functions that are defined as

$$
\begin{aligned}
S_{\mathrm{h}}(k,\omega) &= \frac{1}{\pi}\,\mathrm{Im}\,g(k,\omega), \quad \text{for } \omega \le \epsilon_{\mathrm{F}} \tag{10.5}\\
&= \sum_{\gamma} \left| \langle \Psi_{\gamma}^{(N-1)} | a_k | \Psi_0 \rangle \right|^2 \delta\left(\omega - (E_0^{(N)} - E_{\gamma}^{(N-1)})\right),\\
S_{\mathrm{p}}(k,\omega) &= \frac{1}{\pi}\,\mathrm{Im}\,g(k,\omega), \quad \text{for } \omega > \epsilon_{\mathrm{F}}\\
&= \sum_{\gamma} \left| \langle \Psi_{\gamma}^{(N+1)} | a_k^{\dagger} | \Psi_0 \rangle \right|^2 \delta\left(\omega - (E_{\gamma}^{(N+1)} - E_0^{(N)})\right). \tag{10.6}
\end{aligned}
$$

The single-particle Green's function is then written as

$$
g(k,\omega) = \lim_{\eta \to 0} \left(\int_{-\infty}^{\epsilon_{\mathrm{F}}} \mathrm{d}\omega' \frac{S_{\mathrm{h}}(k,\omega')}{\omega - \omega' - i\eta} + \int_{\epsilon_{\mathrm{F}}}^{\infty} \mathrm{d}\omega' \frac{S_{\mathrm{p}}(k,\omega')}{\omega - \omega' + i\eta} \right). \tag{10.7}
$$

The single-particle Green's function is particularly important since it establishes a direct link to experimental processes that study the effect of a removal or an addition of a particle to the correlated system. As mentioned above, the (e,2e) process is related to the hole spectral function. In addition, the Green's function allows the evaluation of the expectation value for *any* single-particle operator $\hat{O}$ (this is because $\langle \hat{O} \rangle = \sum_{\alpha\beta} \int_{-\infty}^{E_{\mathrm{F}}} \mathrm{d}\omega S_{\mathrm{h}}(\alpha\beta,\omega)\langle\alpha|O|\beta\rangle$ where $\langle\alpha|O|\beta\rangle$ is the matrix representation of $\hat{O}$ in the basis $|\alpha\rangle$). This in turn highlights the importance of single-particle removal or addition spectroscopies, such as single photoemission [27, 28] and (e,2e) processes, which allow insight into the respective part of the Green's function. A further advantage of the Green's function approach is that it offers a systematic way for approximations using the diagram technique [23]. In the diagrammatic expansion for g one introduces the concept of the self-energy Σ [29]. The knowledge of Σ allows the evaluation of g according to the Dyson equation

$$
g(\alpha\beta;\omega) = g_0(\alpha\beta;\omega) + \sum_{\gamma\delta} g_0(\alpha\gamma;\omega)\,\Sigma(\gamma\delta;\omega)\,g(\delta\beta;\omega), \tag{10.8}
$$

where g_0 is the Green's function of a (noninteracting) reference system. The self-energy Σ accounts for all excitations due to the interaction of the particle with the surrounding medium and acts as a nonlocal, energy-dependent, and complex single-particle potential.

10.2.2   The two-particle Green's function

As discussed in detail in Ref. [23], the Dyson equation (10.8) can be derived algebraically and the single particle propagator $g(\alpha t, \alpha' t')$ can be related to the two particle Green's function $g^{\mathrm{II}}(\beta t_1, \beta' t_1', \gamma t_2, \gamma t_2')$. This is a first cycle in a hierarchy that links the N-particle propagator

to the $(N+1)$-particle propagator [30,31]. Of direct relevance to this work is the two-particle propagator $g^{\mathrm{II}}(\beta t_1, \beta' t_1', \gamma t_2, \gamma t_2')$.

Repeating the steps outlined above for the single particle case, one arrives at the Lehmann representation of the two-particle Green's function in terms of energies and states of the systems with N and $N \pm 2$ particles [the $(N-2)$-particle state of the system is achieved upon a $(\gamma,2e)$ reaction]:

$$
g^{\mathrm{II}}(\alpha\beta, \gamma\delta; \Omega) = \sum_n \frac{\langle \Psi_0^{(N)} | a_\beta a_\alpha | \Psi_n^{(N+2)} \rangle \langle \Psi_n^{(N+2)} | a_\gamma^{\dagger} a_\delta^{\dagger} | \Psi_0^{(N)} \rangle}{\Omega - \left[E_n^{(N+2)} - E_0^{(N)}\right] + i\eta}
$$
$$
- \sum_m \frac{\langle \Psi_0^{(N)} | a_\gamma^{\dagger} a_\delta^{\dagger} | \Psi_m^{(N-2)} \rangle \langle \Psi_m^{(N-2)} | a_\beta a_\alpha | \Psi_0^{(N)} \rangle}{\Omega - \left[E_0^{(N)} - E_m^{(N-2)}\right] - i\eta}. \tag{10.9}
$$

Upon analogous considerations made for the one particle case to arrive at the single particle spectral functions, Eqs. (10.5) and (10.6), one can obtain from g^{II} the hole-hole spectral function as $S_{\mathrm{hh}}(\boldsymbol{k}_1, \boldsymbol{k}_1, \Omega) = \mathrm{Im}\, g^{\mathrm{II}}(\boldsymbol{k}_1, \boldsymbol{k}_1, \Omega)$, $\Omega \le 2\epsilon_{\mathrm{F}}/\pi$ which is intimately related to the $(\gamma,2e)$ reaction.

The two-particle Green's function involves two kinds of diagrams: The first type includes two noninteracting single-particle propagators [cf. Eq. (10.8)] and is supplemented by similar diagrams that include all possible self-energy insertions [21]. The second defines the vertex function Γ. The latter involves all generalization of the lowest-order correction to the two-particle propagator in which two particles interact once. To visualize the role of Γ we write g^{II} in the form [21]

$$
\begin{aligned}
g^{\mathrm{II}}&(\alpha t_1, \alpha' t_1', \beta t_2, \beta' t_2')\\
&= i\big[g(\alpha\beta, t_1 - t_2)\, g(\alpha'\beta', t_1' - t_2') - g(\alpha\beta', t_1 - t_2')\, g(\alpha'\beta, t_1' - t_2)\big]\\
&\quad \times \int \mathrm{d}t_a\, \mathrm{d}t_b\, \mathrm{d}t_c\, \mathrm{d}t_d \sum_{abcd} g(\alpha a, t_1 - t_a)\, g(\alpha' b, t_1' - t_b) \tag{10.10}\\
&\quad \times \langle ab|\Gamma(t_a, t_b; t_c, t_d)|cd\rangle\, g(c\beta, t_c - t_2)\, g(d\beta', t_d - t_2').
\end{aligned}
$$

From this equation it is clear that Γ can be considered as the effective interaction between dressed particles. In addition, Γ plays a decisive role in the determination of its single-particle counterpart, the self-energy Σ [21].

In energy-space, the result for the noninteracting (free) product of dressed propagators including the exchange contribution, i. e., the zero-order term of Eq. (10.10) with respect to Γ, reads

$$
\begin{aligned}
g_{\mathrm{f}}^{\mathrm{II}}(\alpha\beta, \gamma\delta; \Omega) &= \frac{i}{2\pi} \int \mathrm{d}\omega \big[g(\alpha, \gamma; \omega)\, g(\beta\delta; \Omega - \omega) - g(\alpha, \delta; \omega)\, g(\beta\gamma; \Omega - \omega)\big]\\
&= \sum_{mm'} \frac{\langle \Psi_0^{(N)} | a_\alpha | \Psi_m^{(N+1)} \rangle \langle \Psi_m^{(N+1)} | a_\gamma^{\dagger} | \Psi_0^{(N)} \rangle \langle \Psi_0^{(N)} | a_\beta | \Psi_{m'}^{(N+1)} \rangle \langle \Psi_{m'}^{(N+1)} | a_\delta^{\dagger} | \Psi_0^{(N)} \rangle}{\Omega - \left\{ \left[E_m^{(N+1)} - E_0^{(N)}\right] + \left[E_{m'}^{(N+1)} - E_0^{(N)}\right] \right\} + i\eta}\\
&\quad - \sum_{nn'} \frac{\langle \Psi_0^{(N)} | a_\gamma^{\dagger} | \Psi_n^{(N-1)} \rangle \langle \Psi_n^{(N-1)} | a_\alpha | \Psi_0^{(N)} \rangle \langle \Psi_0^{(N)} | a_\delta^{\dagger} | \Psi_{n'}^{(N-1)} \rangle \langle \Psi_{n'}^{(N-1)} | a_\beta | \Psi_0^{(N)} \rangle}{\Omega - \left\{ \left[E_0^{(N)} - E_n^{(N-1)}\right] + \left[E_0^{(N)} - E_{n'}^{(N-1)}\right] \right\} + i\eta}\\
&\quad - (\gamma \longleftrightarrow \delta). \tag{10.11}
\end{aligned}
$$

The integration over ω has been carried out by utilizing the Lehmann representation for the single-particle Green's functions. The ladder approximation to the two-particle propagator is then given by:

$$g_L^{II}(\alpha\beta, \gamma\delta; \Omega) = g_f^{II}(\alpha\beta, \gamma\delta; \Omega)$$
$$+ \frac{1}{4}\sum_{\epsilon\eta\theta\zeta} g_f^{II}(\alpha\beta, \epsilon\eta; \Omega)\langle\epsilon\eta|V|\theta\zeta\rangle g_L^{II}(\theta\zeta, \gamma\delta; \Omega), \quad (10.12)$$

where V stands for the naked two-body interaction. This integral relation can now be iterated to yield a set of a ladder diagrams. The corresponding ladder sum for the effective interaction Γ, as it appears in [cf. Eq. (10.10)] can be deduced from this result as

$$\langle\alpha_1, \beta_2|\Gamma_L(\Omega)|\alpha_1', \beta_2'\rangle = \langle\alpha_1 \beta_2|V|\alpha_1' \beta_2'\rangle$$
$$+ \frac{1}{4}\sum_{\epsilon\eta\theta\zeta} \langle\alpha_1 \beta_2|V|\epsilon \eta\rangle g_f^{II}(\epsilon \eta, \theta \zeta; \Omega)\langle\theta, \zeta|\Gamma_L(\Omega)|\alpha_1', \beta_2'\rangle. \quad (10.13)$$

The analogous operators to g_L^{II} and $\Gamma_L(\Omega)$ in absence of the surrounding medium (e. g., as is the case in a dilute gaseous system) are the Green function G and the transition operator T which have been utilized to study multiple ionization of gaseous atomic and molecular targets upon photon and particle impact [32, 33].

As noticed above, g^{II} is of a direct relevance to the $(\gamma, 2e)$ reaction. It should be noted however that the ladder approximation (10.12) for the two-particle Green's function can be employed to define the self-energy Σ [23, 31] which can then be used to obtain the single-particle Green's function via Eq. (10.8). On the other hand, this Green's function enters in the definition of the two-particle Green's function, as clear, e. g., from Eqs. (10.11), (10.12). Thus in principle, the Dyson Eqs. (10.8) and (10.12) for the one-body and two-body Green's functions have to be solved in a self-consistent manner.

As in the single particle case where we established the relevance of the spectral representation to the (e,2e) experiments, one can relate g^{II} to the $(\gamma, 2e)$ measurements by means of Eq. (10.9): g^{II} shows poles at energies (relative to the ground state) corresponding to adding $[E_n^{(N+2)} - E_0^{(N)}]$ or removing $[E_0^{(N)} - E_n^{(N-2)}]$ two particles from the unperturbed ground state. The residua of these poles are related to the measurable spectroscopic factors for the addition or removal of the two particles, e. g., as done in a $(\gamma, 2e)$ experiment. From the above discussion we conclude thus that $(\gamma, 2e)$ and (e,2e) provide quite different information. On the other hand they are related in as much as the single-particle and the two-particle spectral functions are related to each other.

10.3　Photo-induced double-electron emission

Before we implement the expressions in the preceding section into a calculational scheme for the evaluation of the coincident $(\gamma, 2e)$ signal, it is useful to discuss the experimental conditions and limitations.
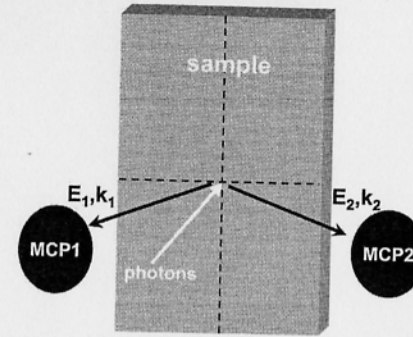
Figure 10.1: The schematic view of the experimental arrangement. The photon beam from the synchrotron source impinges under normal incidence onto the sample, and electron pairs ejected from the sample are detected by two channel-plate assemblies. The center axes of the two detectors are at 40° to the light incidence direction. The sample may be rotated about an axis within its surface, normal to the plane of light and detector axes.

10.3.1　Experimental details

Since double photoemission has a much smaller cross section than single photoemission, detectors with a large acceptance are needed. The method of choice is a time-of-flight technique which allows for a large acceptance both geometrically and in terms of electron energy [13]. By determining the electron energy from the time required by the electron to travel the distance from sample to detector, the large acceptance is achieved without compromising on the energy resolution. In our experiment, we use two time-of-flight spectrometers to detect pairs of electrons ejected from the sample by absorption of one photon (cf. Fig. 10.1). Each detector consists of a pair of 75 mm channel-plates with position sensitive detection via a resistive anode. The detectors are at a distance of 160 mm from the sample, the two detector axes are at ±40° with the light axis. Position sensitive detection is necessary to avoid energy broadening caused by different electron flight distances to the center or edge of the detectors.

Time-of-flight techniques require a pulsed photon source. Pulsed UV photon beams are provided by synchrotron radiation sources, therefore the experiments shown here were performed in the single bunch mode of the electron storage ring BESSY I in Berlin. The repetition frequency of the storage ring in the single bunch mode is 5 Mhz, i.e. the time between two light pulses is 200 ns, and their width is about 0.6 ns. To keep the accidental coincidence rate below or comparable to the real coincidence rate, the mean beam intensity was adjusted such that on average there was less than one photon per bunch.

To obtain the time-of-flight spectrum, the time difference between the photon bunch marker signal delivered by the synchrotron and a fast timing signal provided any of the channel-plate detectors was measured by time-to-amplitude conversion. The overall time resolution achieved in both channels was about 1.2 ns. This yielded an energy resolution of the detected electrons ranging from 0.1 eV for $E_{kin} = 5$ eV to 3.15 eV for $E_{kin} = 50$ eV. The fast timing signals from both detectors were passed to an electronic time-coincidence condition, ensuring that only those events were registered in which two electrons reached the detectors within a time window of 200 ns. As the number of photons per bunch is distributed according to Poisson statistics, a certain number of bunches contained more than one photon. Thus, in addition to correlated electron pairs, one normally detects a background of uncorrelated electrons, i.e., electron pairs generated by two different photons within one bunch. In our experiments this

background was about 15% of the true coincidence rate. For subtracting this contribution from the coincidence spectra, we measured separate background runs by increasing the coincidence window from 200 ns to 1 ms, such that essentially only uncorrelated electron pairs generated by different photon bunches were detected. Before subtraction, the coincidence and background runs were normalized on the integrated single photoemission yield of both runs.

Because of the small escape depth of low energy electrons, the probing depth in an experiment involving the detection of two electrons may be expected to be below 5 monolayers for the energies considered here. Samples are prepared in the usual way by sputtering and annealing of bulk single crystals, sample cleanliness is determined by Auger spectroscopy. The small probing depth allows to investigate materials in the form of thin films deposited on a substrate, which can be considered as representative for the surface of a bulk crystal.

10.3.2   Pathways for the electron-pair emission

For the kind of photons specified in the experimental section, we can treat the electromagnetic field classically and employ the dipole approximation, as shown in detail in Ref. [12]. The electric dipole operator is a sum over single-particle operators. Hence, the photon can be absorbed only by one electron. The other electrons which are emitted in the course of this process have to interact in some way with the photo-excited electron. This is the underlying reason why double photoelectron emission is so sensitive to electronic correlation. In Fig. 10.2 we show the leading Feynman diagrams for the DPE process: In Fig. 10.2(a-b) the two-electron scattering takes place in the initial state (i. e., prior to the photon absorption) via the effective particle-particle interaction. In addition, the photon can excite a collective mode of the system which then decays into two electrons, as schematically shown in Fig. 10.2 (c). Other types of correlations that induce a DPE signal are termed final-state interactions (FSI) [Fig. 10.2(d,e)]. As schematically shown in Fig. 10.2(d,e), one of the ground-state electrons absorbs the photon and then scatters from a second electron. The latter scattering is mediated also by the effective electron-electron interaction. A further important channel for DPE is depicted in Fig. 10.2(f) where one electron absorbs the photon just like in single photoemission (SPE) and undergoes a series of collisions with the crystal potential and with other electrons until it has lost coherence with its initial phase. This photoelectron then scatters from another electron into a two-electron vacuum state. Therefore, the process shown in Fig. 10.2(f) can be considered as product of independent events (cross sections): a single photoemission process followed by an (e,2e) scattering. There is a series of additional diagrams, in particular a combination of the processes represented by Fig. 10.2(a,b) and Fig. 10.2(d,e), i. e., process where the two electrons interact in the initial and the final states. In principle, a division between initial and final state correlation is only a matter of semantics as far as the $(\gamma, 2e)$ process is concerned, as demonstrated by the diagrams in Fig. 10.2(a,b) and Fig. 10.2(d,e): The difference between collisions taking place in the initial or final state is in the time ordering of the electron-electron interaction and the absorption process. This ordering is however of no relevance for the two-photoelectron current $\mathcal{J}$ whose derivation involves an integration over time. In fact, as derived in Ref. [34] $\mathcal{J}$ has the form

$$\mathcal{J} \propto \langle k_1, k_2 | g^{\mathrm{IIr}} \Delta\, S_{\mathrm{hh}}^{\mathrm{II}}(k_1', k_2', E)\, \Delta^{\dagger}\, g^{\mathrm{IIa}} | k_1, k_2 \rangle, \qquad (10.14)$$
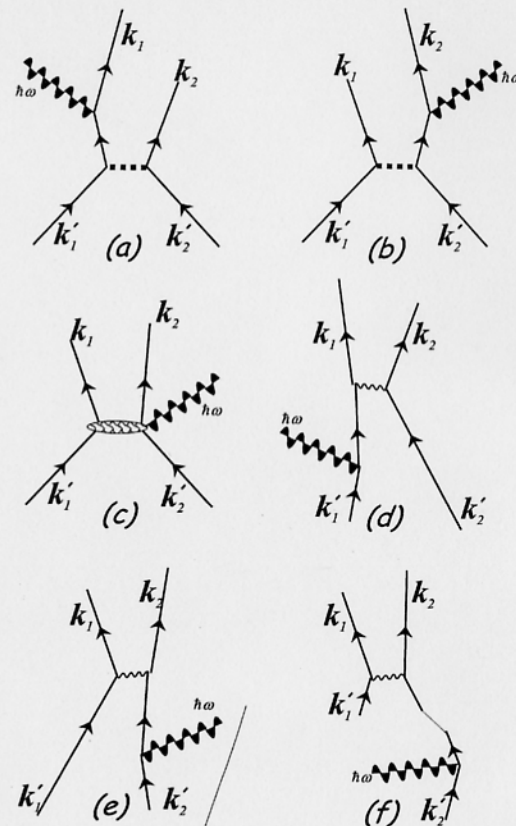
Figure 10.2: The lowest-order Feynman diagrams that contribute to the photo-induced generation of electron-pairs with asymptotic wave vectors k_1 and k_2. The crystal momenta of the two initially bound electrons are denoted by k_1' and k_2'. The thick dotted line indicates an interaction between the electron mediated by the effective electron-electron interaction in the medium whereas the wiggly line symbolize the electron-electron final-state interaction. The photon is indicated by its energy $\hbar\omega$. In inset (c) the photon excites both the electron pair and collective modes of the system. The dotted line in (f) means that the single photoemission process and the subsequent electron-electron scattering take place in two steps and therefore these two processes are incoherent.
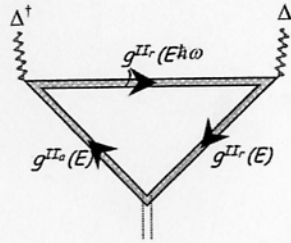
Figure 10.3: Diagrammatic representation of the photocurrent expression Eq. (10.14). Wavy lines represent the photon, double straight lines with arrows correspond to the retarded and advanced two-particle Green's functions as indicated on the plots. The double dashed line symbolizes the electrons emitted into the vacuum.

where Δ is the dipole operator, S_{hh}^{II} is the hole-hole spectral function, and g^{IIa} (g^{IIr}) is the advanced (retarded) two-particle Green's function.

Similar to the case of single photoemission, the photocurrent can be represented by the two-particle Caroli diagram, as shown in Fig. 10.3, which explicitly shows no signature of time ordering. On the other hand, one can tune to initial or final state correlation by choice of the wave vectors that appear in the current expression Eq. (10.14): If k_1 and k_2 are very large (compared to the Fermi wave vector), one can expect the final-state interactions to be limited to a small region in phase space where the two electrons escape with almost the same velocities. Apart from this regime, FSI become less important which allows to highlight the effect of initial-state correlations. On the other hand, if the two electrons escape with very low (vacuum) velocities, FSI become the determining factor. These statements will be illustrated below with numerical examples.

10.4   Numerical realization and experimental results

As is clear from Eq. (10.14), the evaluation of g^{II} is the key ingredient for the numerical evaluation of the two-photoelectron current. On the other hand, we have seen in the preceding section that the single-particle Green's function g is needed to obtain g^{II}, and in turn g^{II} goes into the determination of g. Till now this self-consistent loop has been too complicated to be realized numerically within a realistic description of the surface, i. e., for an inhomogeneous electron gas. In fact, the exact evaluation of the generally valid Eq. (10.14) is still an open question even for a system of few interacting charged particles, such as a few-electron atom. This kind of systems is currently subject of active research, with DPE being the principle tool to uncover the effect of particle-particle correlations and to test the validity of various numerical suggestions for the evaluation of Eq. (10.14). For a recent reviews on this topic, we refer to Refs. [15–19]. In the present case, we need to account for the few-particle scattering in the presence of the surrounding inhomogeneous system of electrons.

10.4.1   Simple model calculations

The effect of the medium on the electron-electron interaction V can be estimated for the case of a semi-infinite homogeneous electron gas in the long-wavelength regime (Thomas-Fermi
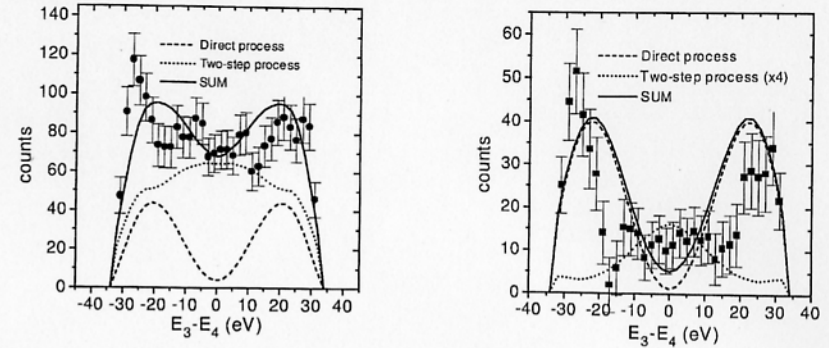
Figure 10.4: $(\gamma,2e)$ energy-sharing distributions from Cu(001) (left-hand panel) and Ni(001) (right-hand panel) due a 45 eV photon incident normal to the surface. The experimental data ([13, 14]) are for electron pairs with sum energies $E_1 + E_2$ between 33 eV and 35 eV. The two photoelectrons are emitted at $40°$ symmetrically to the left and to the right of the surface normal. The theoretical curves show the coherent contributions from the diagrams depicted in Fig. 10.2(d,e) (dashed lines) whereas the dotted line indicate the results for the cross section obtained from the process shown in Fig. 10.2(f) (for the Cu case the dotted curve has been scaled up by a factor of 4 for visibility). The solid line is the summed cross section, i.e. the incoherent sum of the dotted and dashed lines.

limit). In this case, V is well described by the modified, local potential U where [35]

$$U = \frac{e^{-(|r_1-r_2|)/\lambda}}{|r_1 - r_2|}. \tag{10.15}$$

Here, $r_1 - r_2$ is the relative distance between the two electrons. The screening length λ is related to density of states at the Fermi level. With the electron-electron interaction potential, the first order term in the ladder approximation for g^{II} has been employed and the photocurrent has been evaluated taking into account the diagrams shown in Fig. 10.2 (d,e,f) [cf. Eqs. (10.12) and 10.14]. It should be stressed here that the diagrams Fig. (10.2) (d,e,f) should be calculated within the same model, in which case the relative contributions of each of these processes can be determined.

Figure 10.4 shows measured and calculated two-electron energy correlation functions. The two electrons have a fixed total energy of 35 eV this energy is chosen such that the two electrons are emitted from the vicinity of the (two-particle) Fermi level. Results are shown for the (001) surfaces of Cu and Ni. The material properties within the theory enters via the density of state which determines the screening length and via the characteristics of the surface potentials. As shown in Ref. [12], the present model predicts that the two-photoelectron current can be cast into the form $\hat{\epsilon} \cdot (k_1 + k_2) L$, where L is a complicated function of the electrons' wave vectors and energies. $\hat{\epsilon}$ is the polarization vector of the light. Hence, for $k_1 = -k_2$ or for $\hat{k}_1 \perp \hat{\epsilon} \perp \hat{k}_2$ the cross section vanishes. This is the origin of the minima for equal

energy sharing, as observed in Fig. 10.4. This figure also indicates that the diagrams shown in Fig. 10.2(f) and Fig. 10.2(d,e) deliver comparable contributions to the total current, which is comprehensible, as all of these diagrams involve the same order of the electron-electron and electron-photon interactions.

10.4.2   Numerical scheme with a realistic single-particle band structure

To improve on the above two-particle interacting jellium model, while taking into account the electron-electron interaction explicity and treating the two photoelectrons on equal footing, we proceed as follows: If we assume the two photoelectrons to be independent, then, according to Eq. (10.12), the two-particle Green's function g^{II} reduces to $g^{II} = g_t^{II}$. This means g^{II} simplifies to an anti-symmetrized product of single-particle Green's function $g_j(k_i, E_i)$, $i = 1, 2$, which can be used to generate the single-photoelectron states. Employing the one-step model for photoemission we can then calculate the single-photoelectron current. Our approach towards this single-particle problem is based on the layer Korringa-Kohn-Rostoker (LKKR) method which utilizes a density-functional approach combined with an empirical function for the complex part of the self-energy. This single-particle part of the problem is essentially the same as in the case of as in single photoemission [36, 37] and (e,2e) which has been reviewed in details in the chapter by Feder and Gollisch of this volume. Therefore we focus here on how the two independent photoelectron currents can be coupled to evaluate a finite two-electron photocurrent $\mathcal{J}$ (we recall that $\mathcal{J}$ vanishes in absence of correlations].

For this purpose, we utilize the interaction potential U, defined by Eq. (10.15), as a starting point and rewrite it in the following form:

$$U = \frac{Z_1}{r_1} + \frac{Z_2}{r_2} \quad \text{with} \quad Z_j = a_j^{-1} \exp\left(-\frac{2a_j}{\lambda} r_j\right), \qquad j = 1, 2. \tag{10.16}$$

In these relations, we have introduced the functions $a_j = r_{12}/(2r_j)$. Equation (10.16) can be interpreted in the following way: The effect of the electron-electron interaction potential can be viewed as a modification Z_j/r_j to the single-particle potentials. This means that the inter-electronic correlation is subsumed into a dynamic nonlocal screening interaction w_j of the electron with the lattice. The behaviour of this screening is dictated by the functions Z_j, and has the following features: When the two electrons are on top of each other ($r_{12} \to 0$) the potential w_j turns repulsive as to simulate the strong, short-range electron-electron repulsion. If the two electrons are far away from each other ($r_i \gg r_j$, $i \neq j \in [1, 2]$), the screening strengths Z_1 and Z_2 become negligible and we end up with two independent particles. It should be stressed that, within our model, the dynamic screening as introduced in Eq. (10.16) is exact, since we merely performed rearrangements of the interactions involved in Eq. (10.15). Hence, the evaluation of the two-photoelectron current will face the same problems as when Eq. (10.15) is utilized. To circumvent the numerical difficulties we approximate the dynamical screening strengths Z_j by $\bar{Z}_j$ where $\bar{Z}_j = \bar{a}_j^{-1} \exp\left(-2\bar{a}_j r_j/\lambda\right)$ and $\bar{a}_j = k_{12}/(2k_j)$. Here $k_{12} = k_1 - k_2$ is the inter-electronic relative wave number. This approximation is valid, if, e. g., $r_j \propto k_j$. In other words, the *potential* (10.15) is exactly diagonalized when the particles proceed along trajectories satisfying the relation $\mathbf{r}_j \propto k_j$, e. g., uniform orbits. With this screening being included, the modification $\bar{Z}_j/r_j$ to the original single-particle potential w_j can be taken into account and the single-particle Green's function $\bar{g}_j$ is generated. However,

in contrast to g, each $\bar{g}_j$ is dependent on the wave vectors of *both* electrons as well as on the mutual, relative wave vector of the escaping electrons. The two-particle Green's function is approximated by $\bar{g}^{II}$ which is the anti-symmetrized, direct product of the modified single-particle Green's functions $\bar{g}_j$ (the first term in the ladder approximation, Eq. (10.12)). With this model reasonable results have been obtained for the (e,2e) cross sections [11, 38, 39].

10.4.3   Numerical results for the angular pair correlation in Cu(001)

We discuss in this section pilot results for the correlated two-photoelectron current from a clean Cu(001) surface. Only the diagrams shown in Fig. 10.2(d,e) have been evaluated. The ground-state potentials have been calculated self-consistently with the scalar-relativistic LMTO method. Life-time broadening of the spectra was simulated by employing a complex optical potential. The photoelectrons' current due to emission from the first 20 outermost layers was calculated. Convergence of the results with respect the maximum angular momentum, number of reciprocal lattice vectors, and accuracy of the energy integration has been achieved.

To get an insight into the profound difference between single and double-photoelectron emission, we compare in Fig. 10.5 the angular distribution of the photoelectron currents for single photoemission (labeled SPE) and the double photoemission (indicated by DPE) for an incoming s-polarized photon. The intensity variation is shown as function of the angular position of one photoelectron with 9 eV kinetic energy. The photon energy is 15.5 eV in the single photoemission case and 31 eV for double photoemission. We note that in the latter case both photoelectrons escape with the same kinetic energy of 9 eV.

In single photoemission, the point group of the surface $4mm$ is reduced to $2mm$ in the angular distribution (as indicated by the horizontal and vertical lines in Fig. 10.5) because the electric-field vector of the incident photon (which lies in a mirror plane of the surface) is not invariant under the operations C_4 and C_4^{-1}. On the other hand in double photoelectron emission, the group $2mm$ is reduced further to m (horizontal line in Fig. 10.5). This is due to the presence of the second photoelectron whose emission direction is fixed in space and is indicated on the plot by the small circle.

The influence of the correlation between the two photoelectrons is readily visible Fig. 10.5: The repulsion between the two escaping photoelectrons leads to a vanishing photoelectron current when the two electrons are close to each other. This is the origin of the *correlation hole* surrounding the fixed detector position. On the other hand, if the two electrons are far from each other, the electron-electron interaction diminishes in strength. Consequently, the two-electron current drops dramatically, for this current must vanish in absence of correlation. The interplay between these two effects leads to a 'localization' of the angular intensity distribution of one of the photoelectrons around the position of the second one, as observed in Fig. 10.5. It should be stressed that the two detected photoelectrons are not only coupled to each other via the interaction (10.15) but also to the crystal potential. Therefore, the *correlation hole* is not isotropic in space and depends sensitively on the photoelectrons' energies.

To illustrate the dependence of the *correlation hole* on the short-range components of the electron-electron interaction, we recall that the strength of the electron-electron scattering potential (10.15) is primely determined by the screening length λ, which depends on the density of state. Therefore, for the sake of demonstration, we can regard λ as a parameter and study the correlation between the two-photoelectron current and the value of λ. This is depicted

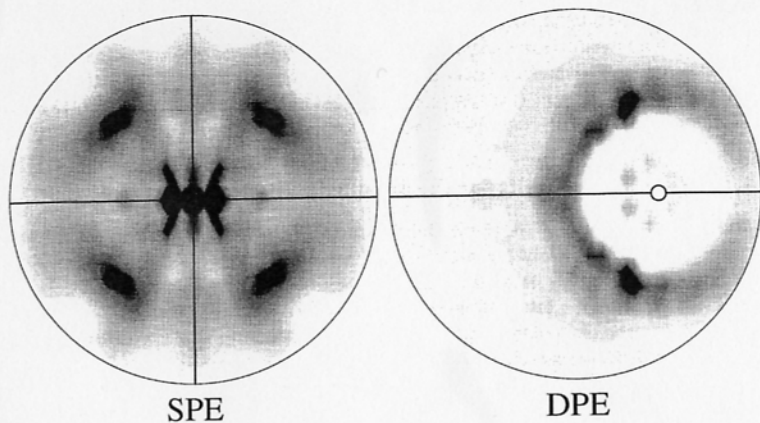SPE   DPE

Figure 10.5: Angular distribution of the photoemission intensity from Cu(001) in single-electron (la-beled SPE) and double-electron photoemission (labeled DPE). The kinetic energy of the photo-electrons is 9 eV, the photon energy of the s-polarized light 15.5 eV in the SPE case whereas in DPE the photon energy is increased to 31 eV as to compensate for the additional energy needed to emit two electrons instead of one. For the DPE case, the small circle indicates the emission direction of one of the detectors (polar angle with respect to the surface normal is $\vartheta = 40°$). Low (high) intensities correspond to light (dark) gray scale in the stereographic projection. Horizontal and vertical lines emphasize the symmetries of the angular distributions.

in Fig. 10.6 which evidently shows that the correlation length λ is intimately related to the two-photoelectron current. In fact, an angular measurement of the kind shown in Fig. 10.6 can provide an estimate of the correlation length λ in the material under study.

The difference between Fig. 10.6 and Fig. 10.5 is that the photoelectrons' kinetic energies are increased from 9 eV for each electron in Fig. 10.5 to 15 eV for each electron in Fig. 10.6. As clear from the calculations shown in these figures the extent of the correlation hole shrinks considerable when the electrons' energies are increased. In fact, at extremely high energies, the two electrons interact only in a very limited region when they are emitted in the same directions and their velocities are comparable. This can be deduced directly from the interaction potential (10.16).

10.4.4   Energy-correlation functions

In the preceding section we discussed the mutual angular correlation between the two photo-electrons escaping with well-defined energies. Now, we study the energy electron-pair corre-lations at a fixed angular position of the emitted electrons. This is done in Fig. 10.7 where we present the two-photoelectron current from Cu(001) as a function of electrons' energies E_1, E_2 for a fixed photon energy (p-polarized light) and fixed angles of emission. Again, only
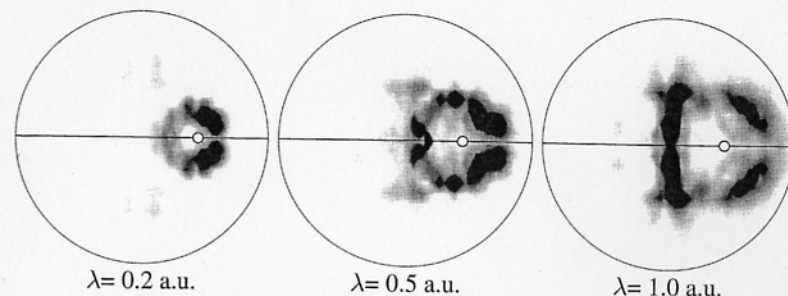
$\lambda = 0.2$ a.u. $\lambda = 0.5$ a.u. $\lambda = 1.0$ a.u.

Figure 10.6: The effect of the correlation length λ on the angular distribution of the two-photoelectron current from Cu(001). The photon is s-polarized and has an energy of 45 eV. The photoelectrons have equal kinetic energies of 15 eV. The angular arrangement of the detection geometry is as in Fig. 10.5. The stereographic images show angular distributions for $\lambda = 0.2$ a.u. (left), 0.5 a.u. (middle), and 1.0 a.u. (right). The horizontal lines emphasize the mirror symmetry of the angular distributions.
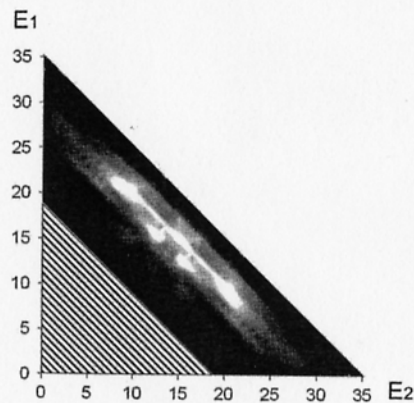

Figure 10.7: The two-photoelectron current as a function of energies E_1, E_2 of the two pho-toelectrons. Black and white contrasts corre-spond to low and high intensities, respectively. The emission angles of the electrons are fixed at $\theta = 30°$ symmetrically to the left and right of the surface normal. The photon energy is $\omega = 45$ eV. The shaded triangle indicates the re-gion below the bottom of the conduction band.

the diagrams depicted in Fig. 10.2 (d,e) have been taken into account. As in the case of the an-gular distribution, we notice that the photoelectron current is appreciable in the region where the two electrons can interact efficiently. According to our interaction potential (10.16), this is the case when the two electrons do not differ too much in their kinetic energies. This is reflected in the behaviour of the photoelectrons current as observed in Fig. 10.7.

From Fig. 10.7 we also notice that the photoelectron current (white region) originates basically from the energy region $E_1 + E_2 = E = 25 \cdots 35$ eV, where E is the total kinetic energy of the pair. From energy conservation it is readily concluded that this energy interval corresponds to the d-band of copper (≈ 3 eV band below the Fermi level) from which the initial state electrons originate mostly; only a negligible fraction of electron pairs are emitted in the

region $E < 25$ eV and in the narrow black band just below the line marked by the $E = 35$ eV. This is due to the low density of the initial states in these configurations. It should be noted in this context that in Fig. 10.7 we basically scan the two-photoelectron current through the conduction band starting at the Fermi level (correspond to $E \approx 35$ eV) and ending at the bottom of the conduction band (which is at $E \approx 18$ eV). In this case it is very important to account (e.g. via a realistic self-energy function) for additional multiple elastic and inelastic scattering processes of the electrons pairs [29]. In the calculations shown in Fig. 10.7 it has not been yet possible to include this kind of additional processes. This limitation of theory is however not applicable to the angular distribution results shown in Fig. 10.5, since in this case the energy of the electrons can be chosen such that the photoelectrons are emitted from the Fermi level where inelastic energy-loss processes can be deemed small.

10.5   Conclusions

The aim of the present work is to provide a general overview of the foundations and of the numerical methods for describing the photo-induced two-electron emission from surfaces. A brief account of the experimental techniques have been given and the experimental data have been discussed in light of the numerical results. We have seen that the double photoelectron emission is well suited for the study of particle-particle correlation in a very direct way, i.e., in actually detecting the two particles at the same time. A general expression has been given to evaluate the $(\gamma, 2e)$ current and some approximate calculation schemes have been outlined. In particular, we employed a local but wave-vector dependent approximation of the electron-electron interaction between the photo-electrons and established a multiple-scattering scheme which is closely related to the well-studied one-step model of single photoemission. In particular, we can treat within the same numerical approach single and double-photoelectron emission which allows for a reasonable comparison between the two processes. First numerical results for the angular and the energy correlation functions of the photoelectrons emitted from Cu(001) revealed the characteristics of the electronic correlation, as can be observed in $(\gamma, 2e)$. Future improvements of the present approximate model include the implementation of a realistic single-particle self energy in the one-particle part of the problem as well as taking explicitly into account the non-local screened Coulomb interaction.

References

[1] P. Fulde, *Electron Correlation in Molecules and Solids*, Springer Series in Solid-State Sciences, Vol. 100, Springer Verlag, 1991.

[2] R.M. Dreizler and E.K.U. Gross, *Density Functional Theory*, Springer Verlag, 1990.

[3] I. Lindgren and J. Morrison, *Atomic Many-Body Theory*, Springer Verlag, 1982.

[4] K.A. Brueckner, Phys. Rev. **97** (1955) 1353.

[5] H.A. Bethe, Ann. Rev. Nucl. Sci. **21** (1971) 93.

[6] J.P. Jeukenne, A. Legeunne, and C. Mahaux, Physics Reports **25** (1976) 83.

[7] H. Kümmel, K.H. Lührmann, and J.G. Zabolitzky, Physics Reports **36** (1978) 1.

[8] R.F. Bishop, in *Microscopic Quantum Many-Body Theories and Their Applications*, eds. J. Navarro and A. Polls, Springer, 1998.

[9] K.E. Schmidt and D.M. Ceperley, in *Monte Carlo Methods III*, ed. K. Binder, Springer, 1991.

[10] D.M. Ceperley, Rev. Mod. Phys. **67** (1995) 279.

[11] R. Feder and H. Gollisch, this volume.

[12] J. Berakdar, Phys. Rev. B **85** (1998) 9808.

[13] R. Herrmann, S. Samarin, H. Schwabe, and J. Kirschner, Phys. Rev. Lett. **81** (1998) 2148.

[14] R. Herrmann, S. Samarin, H. Schwabe, and J. Kirschner, J. Phys. (Paris) IV, **9** (1999) 127.

[15] J. Berakdar, and J. Kirschner, eds. *Many-Particle Spectroscopy of Atoms, Molecules, Clusters and Surfaces*, Kluwer Acad/Plenum Pub., 2001.

[16] J.S. Briggs and V. Schmidt, J. Phys. B **33** (2000) R1.

[17] G.C. King and L. Avaldi, J. Phys. B **33** (2000) R215.

[18] V. Schmidt, *Electron Spectrometry of Atoms using Synchrotron Radiation*, Cambridge Monographs on Atomic, Molecular and Chemical Physics Cambridge, University Press, 1997.

[19] J. Berakdar and H. Klar, Phys. Rep. **340** (2001) 473.

[20] C.J.G. Onderwater *et al.*, Phys. Rev. Lett., **81** (1998) 2213.

[21] A.L. Fetter and J.D. Walecka, *Quantum Theory of Many Particle Systems*, McGraw-Hill, New York, 1971.

[22] G.D. Mahan, *Many-Particle Physics*, second ed., Plenum Press, London, 1993.

[23] A.A. Abrikosov, L.P. Gorkov and I.E. Dzyaloshinski, *Methods of Quantum Field Theory in Statistical Physics*, Dover, 1975.

[24] J. Negele and H. Orland, *Quantum Many-Particle Systems*, Addison-Wesley, 1988.

[25] R.D. Mattuck, *A Guide to Feynman Diagrams in the Many-Body Problem*, McGraw-Hill, 1976.

[26] H. Lehmann, Nuovo Cimento A **11** (1954) 342.

[27] S.D. Kevan (Ed.), *Angle-Resolved Photoemission: Theory and Current Application*, Elsevier, 1992.

[28] S. Hüfner, *Photoelectron Spectroscopy*, No. 82 in Springer Series in Solid-State Science, Spinger Verlag, 1995.

[29] L. Hedin, J. Phys. C **11** (1999) R489.

[30] P.C. Martin and J Schwinger, Phys. Rev. **115** (1959) 1342.

[31] A.B. Migdal, *Theory of finite Fermi Systems*, New York, 1967.

[32] J. Berakdar, Phys. Rev. Lett. **85** (2000) 4036.

[33] J. Berakdar, Phys. Rev. A **63** (2001) 012706.

[34] N. Fominykh, J. Henk, J. Berakdar, P. Bruno, H. Gollisch, R. Feder, Solid State Commun., **113** (2000) 665.

[35] D. Pines, *The Many-Body Problem*, Bejamin, 1962.

[36] R. Feder (Ed.), *Polarized electrons in surface physics*, Advanced Series in Surface Science, World Scientific, 1985.

[37] J. Henk, in *Handbook of Thin Film Materials* (ed.) H.S. Nalwa, Academic Press, 2001.

[38] J. Berakdar, H. Gollisch and R. Feder, Solid State Commun. , **112** (1999) 587.

[39] N. Fominykh *et al.*, in *Many-particle spectroscopy of Atoms, Molecules, Clusters and Surfaces*, Kluwer Acad/Plenum Pub., 2001.